

PAPER

Gold nanodome SERS platform for label-free detection of protease activity

Pieter C. Wuytens,^{id}*^{abc} Hans Demol,^{fg} Nina Turk,^{id}^{acd} Kris Gevaert,^{fg} Andre G. Skirtach,^{bc} Mohamed Lamkanfi^{de} and Roel Baets^{ac}

Received 10th April 2017, Accepted 23rd June 2017

DOI: 10.1039/c7fd00124j

Surface-enhanced Raman scattering provides a promising technology for sensitive and selective detection of protease activity by monitoring peptide cleavage. Not only are peptides and plasmonic hotspots similarly sized, Raman fingerprints also hold large potential for spectral multiplexing. Here, we use a gold-nanodome platform for real-time detection of trypsin activity on a CALNNYGGGGVGRGNF substrate peptide. First, we investigate the spectral changes upon cleavage through the SERS signal of liquid-chromatography separated products. Next, we show that similar patterns are detected upon digesting surface-bound peptides. We demonstrate that the relative intensity of the fingerprints from aromatic amino acids before and after the cleavage site provides a robust figure of merit for the turnover rate. The presented method offers a generic approach for measuring protease activity, which is illustrated by developing an analogous substrate for endoproteinase Glu-C.

Introduction

Proteases, which are enzymes that catalyse the hydrolysis of peptide bonds, play a crucial role in the modification of proteins and in the breakdown of proteins into their constituent amino acids (protein catabolism). Furthermore, proteases are of vital importance in numerous signalling pathways.¹ Sensitive and quantitative analysis of protease activity is of critical importance for, amongst other things, medical diagnostics,² drug development¹⁻³ and single cell analysis.^{4,5} As over 500 different genes encoding for proteases have been identified in the human genome, there is large interest in a detection technology that allows for a selective, sensitive and multiplexed measurement of protease activity. Current established methods such as colorimetric or fluorescent assays and liquid chromatography lack

^aPhotonics Research Group, INTEC, Ghent University – imec, Belgium. E-mail: pieter.wuytens@ugent.be

^bDepartment of Molecular Biotechnology, Ghent University, Belgium

^cCenter for Nano- and BioPhotonics, Ghent University, Belgium

^dCenter for Inflammation Research, VIB, Belgium

^eDepartment of Internal Medicine, Ghent University, Belgium

^fVIB-UGent Center for Medical Biotechnology, Belgium

^gDepartment of Biochemistry, Ghent University, Belgium

sensitivity or are not scalable to real-time, multiplexed assays. In recent years, several strategies based on nanoparticle–peptide complexes^{6–8} have been developed for detecting protease activities. These are typically based on fluorescence-quenching or -energy transfer, offering high sensitivity in *in vitro* and even *in vivo* measurements. However, fluorescence-based methods provide limited multiplexing capabilities. In contrast, the specificity of Raman fingerprints enables spectrally multiplexed measurements.⁹ Furthermore, surface-enhanced Raman scattering (SERS) provides a promising technology for sensitive and selective detection of peptide bond hydrolysis because the nanometer-sized peptides match well with the typical size of a plasmonic hot-spot. Not surprisingly, a number of studies reported on detecting protease activity based on SERS^{10–14} and surface-enhanced resonance Raman scattering (SERRS).^{15–17} These include indirect sensing methods based on clustering¹⁴ and anti-clustering¹³ of nanoparticles upon cleavage, and direct detection methods based on appearances¹⁷ and disappearances^{10,11} from the spectra of SERS labels. These studies demonstrate the ability of detecting protease activities at single-cell concentration levels in sub-nL volumes.^{11,13,15}

In this manuscript, we show real-time detection of trypsin-mediated peptide bond hydrolysis through the SERS spectra of surface-bound peptides consisting of only natural amino acids. We use the inherent SERS fingerprint of aromatic amino acids^{18,19} in our peptides, which eliminates the use of fluorescent- or SERS-labels. As a consequence, the peptide design is easily adjustable towards a specific substrate† for different proteases. These peptides form a self-assembled monolayer²⁰ on a gold-nanodome patterned SERS platform,²¹ with distinguishable vibrational spectra both before and after the cleavage site. This enables discriminating protease activity at a specific cleavage site from ligand exchange.^{22,23} We take a stepwise approach to prove that the changes in the SERS spectra upon peptide hydrolysis indeed originate from substrate cleavage. First, Raman spectra of the pure peptide are compared to SERS spectra acquired on the nanodome surface. Peaks are attributed to known vibrations in the literature and to our own experimental data. Next, we investigate the SERS spectra of the cleaved products separated by reverse phase high-performance liquid chromatography (RP-HPLC) after incubating specific substrates with the serine proteases trypsin and endoproteinase Glu-C. We also verify that the peptides are bound to the nanodome gold surface through an amine-terminal cysteine, correctly presenting the cleavage site away from the solid interface. Finally, we demonstrate digestion of a surface-bound trypsin substrate and follow this reaction in real-time through continuous changes in the SERS spectra.

Results and discussion

Measurement principle and design of the peptide substrate

Fig. 1(a) shows the experimental concept. A monolayer of peptides containing a specific cleavage site was bound to a gold nanostructure. This monolayer

† The term 'substrate' is confusing in the context of SERS for protease sensing. During protease activity, a substrate is the material upon which the protease acts. Here, this is the peptide chain that is converted from a substrate into products upon digestion by the protease. In the field of SERS, a substrate refers to the nanostructured surface that provides a localized surface-plasmon resonance responsible for the enhancement. In this paper, the word substrate is used for the peptide chain. We refer to the nanostructured surface as a SERS platform.

provides a SERS signature from amino acids both before and after the cleavage site. After protease digestion, the part of the SERS spectrum originating from the cleaved-off, non-surface bound product decreases, while the products attached to the gold surface provide a steady signal. Although the measurement principle is fairly straightforward, a correct design of the peptide is crucial for efficient protease digestion and sensitive SERS detection. The peptides should form a stable monolayer on a gold surface, provide an accessible cleavage site and include strong SERS scatterers. Furthermore, the total length of the molecule must remain limited to a few nanometers because of the decreasing SERS signal with increasing distance.^{24,25} Fig. 1(b) shows the proposed peptide in more detail, designed as a specific substrate for trypsin digestion. From the amine- to carboxyl-terminus, it starts with the pentapeptide CALNN.^{20,22,23,26} In this part, the cysteine (C) ensures a covalent sulphur–gold bond.²⁷ The hydrophobic amino acids alanine (A) and leucine (L) help to form a self-assembled monolayer, followed by a double hydrophilic asparagine (N) to ensure good solubility.²⁰ CALNN is followed by tyrosine (Y), an aromatic amino acid that serves as a first SERS reporter. If present, its SERS signature confirms that the CALNNY fraction is still bound to the gold surface, meaning that there has not been any ligand exchange,²⁸ desorption or non-specific cleavage in this part. Next, a stretch of glycines (GGGG) is included, small amino acids forming a flexible chain to improve the accessibility for the protease to the cleavage site. We experimentally found that the presence of this additional spacer is crucial for trypsin activity on surface-bound peptides. These glycines are followed by VR being respectively the P₂ and P₁ subsite for trypsin. It is well known that trypsin cleaves at the carboxyl side of arginine (R) and lysine (K).²⁹ The hydrophobic valine (V) in a P₂ position further increases the efficiency of the catalysis.³⁰ The cleavage site is followed by a GNF sequence. The small glycine at P'₁ ensures good accessibility of trypsin to the cleavage site. The hydrophilic asparagine helps the solubility of the end-fraction of the peptide and, finally, the second aromatic amino acid phenylalanine (F) functions as a second SERS reporter. As a consequence, for this specific substrate the intensity of F-related peaks divided by that of Y-related peaks in the SERS spectrum (I_F/I_Y) gives a metric for the cleavage and diffusion of the –GNF fraction.

An analogous peptide substrate for a different protease was fabricated by adjusting the specific cleavage site. Placing the amino acids NNE– in the P₃–P₁ and –SWH in the P'₁–P'₃ positions (Fig. 4(b1)) makes the substrate suited for hydrolysis by endoproteinase Glu-C, which cleaves the peptide bond C-terminal to glutamic acid (E) residues.³¹ Tryptophan (W) serves here as an aromatic reporter in the cleaved-off fraction, resulting in a different SERS spectrum that allows I_W/I_Y to be used as a metric for endoproteinase Glu-C digestion. Thus, the generic design of the peptide substrate provides the ability to use this technology in different applications, and has the potential for simultaneously monitoring the activity of different proteases on different substrates.

The nanodome SERS platform as a compromise between accessibility and enhancement

For most applications, the ideal SERS platform provides a strong, uniform field-enhancement and has good batch to batch reproducibility. For the specific case of sensitive and quantitative monitoring of protease activity, the field

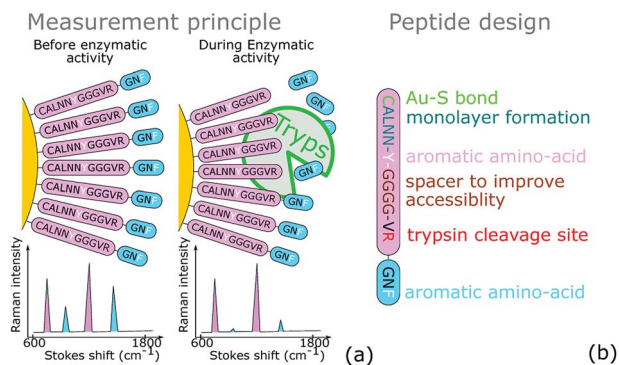


Fig. 1 (a) A gold-bound peptide substrate provides a SERS fingerprint with distinctive peaks from amino acids on both sides of the cleavage site. After protease hydrolysis, the non-bound product diffuses away and its Raman peaks disappear. (b) The peptide substrate designed for trypsin hydrolysis, which cleaves C-terminal to arginine (R) residues.

enhancement has to stretch a few nanometers from the gold surface and the hotspots have to be accessible. The latter is of crucial importance, as most proteases have a molecular weight of 20–50 kDa, roughly corresponding to a Stokes radius of 2–3 nm.³² One can easily imagine that a peptide substrate located in a <5 nm wide hotspot is inaccessible for a trypsin (23 kDa) or endo-proteinase Glu-C (27.7 kDa) molecule. Fortunately, pore sizes starting from 10 nm are accessible to enzymes in this size range.³³ The requirements described above are to a certain degree contradictory. Isolated nanostructures such as nanorods or nanotriangles provide optimal accessibility, but exhibit a low enhancement factor and a stronger distance-dependence as compared to coupled geometries. On the other hand, superior surface-enhancement is achieved in coupled nanostructures with a sub-5 nm, poorly accessible gap.³⁴ To address these concerns, we fabricated gold-nanodome structures²¹ with a gap (g) of 10–15 nm. Fig. 2 shows the fabrication flow and corresponding SEM images of these nanodome patterned chips, processed on 4'' wafers using nanosphere-

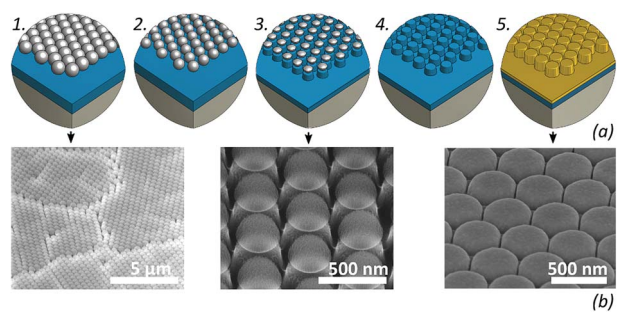


Fig. 2 (a) Schematic and (b) corresponding tilted SEM figures of the fabrication of a gold-nanodome structured surface. A monolayer of polystyrene beads (1–2) forms a mask for reactive ion etching into the underlying Si₃N₄ (3–4), resulting in an array of nanopillars serving as a template for gold deposition (5).

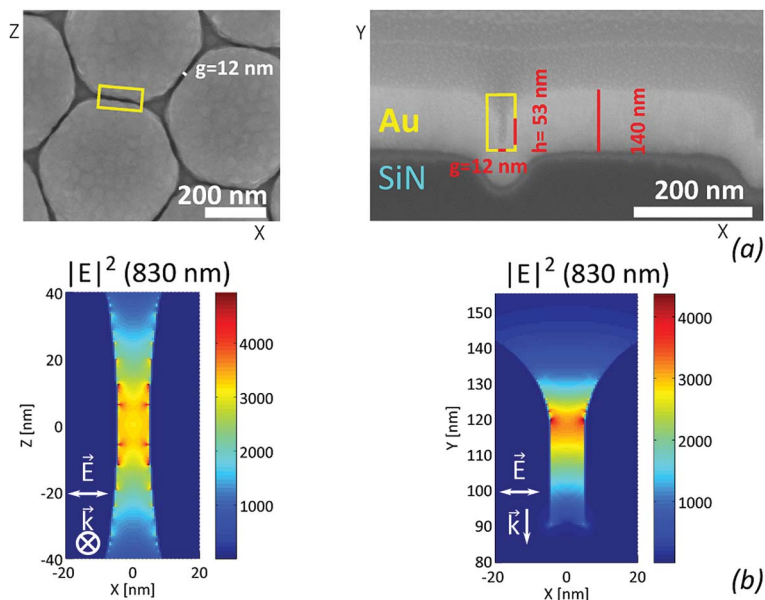


Fig. 3 (a) Top-down and cross-section SEM images for a nanodome-patterned chip with a 12 nm wide (g) and 53 nm high (h) inter-dome gap. (b) Corresponding $|E|^2$ field distributions for this geometry at resonance wavelength simulated through 3D FDTD, showing that the localized surface plasmonic resonance is confined to the inter-dome gap region. The field distributions are plotted over the region corresponding to the yellow rectangles.

lithography. This fabrication method provides ample chips at a reasonable cost and effort. It avoids using e-beam lithography¹¹ while offering superior control on the hotspot size and enhancement factor as compared to colloidal approaches.³⁵ The localized surface-plasmon resonance of these nanodome structures was optimized through UV-Vis reflection and SERS measurements for an optimal enhancement with a 785 nm Raman pump laser and 600 cm^{-1} to 1700 cm^{-1} Stokes shifts in a water environment. Fig. 3(a) shows the resulting geometry with a gap width (g) of 12 ± 2 nm and a height (h) of 53 ± 4 nm. We experimentally measured a SERS substrate enhancement factor (SSEF,³⁶ see the Experimental section) of $1 \pm 0.2 \times 10^6$ for the chips used in this manuscript. The coefficient of variation (σ/μ) on the SERS signal across a single chip is 6–7%. For comparison, we measured a maximum SSEF of 6×10^6 in the nanodome structures with a gap width of approximately 6 ± 2 nm, unlikely to have good accessibility to the peptide substrate in the hotspots. Note that SSEF is a figure for the surface-enhancement per molecule averaged across the gold surface. The surface area of the hotspots accounts for approximately 10–15% of the total gold surface area, calculated from the SEM images in Fig. 3(a). Thus, for molecules in this region, the SERS hotspot enhancement factor (SHEF) is of the order of 10^7 , which is in correspondence with the 3D FDTD simulated electric field profile (Fig. 3(b)) in a $|E|^4$ approximation. These field profiles also show that the LSPR stretches across the full width of the gap. Assuming a loading density of 2 peptides per nm^2 ,^{26,28} there are roughly 10^4 peptides per hotspot.

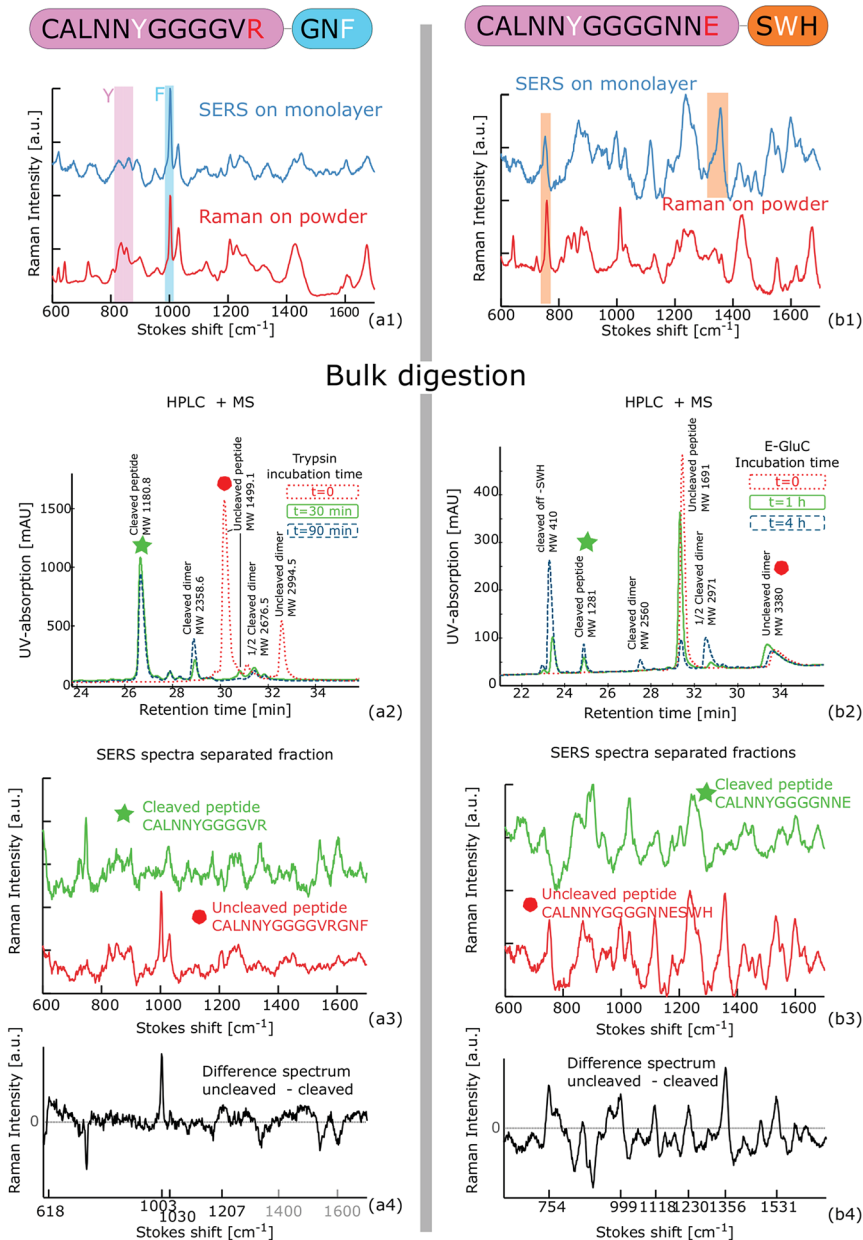


Fig. 4 (a1) Raman and SERS spectra of the CALNYYGGGGVGR trypsin substrate show characteristic tyrosine and phenylalanine peaks. (a2) RP-HPLC was performed after incubation of this peptide with trypsin and the eluting peaks were analysed by mass spectrometry which shows almost full digestion after 30 minutes of incubation with trypsin. (a3) The SERS spectra of the RP-HPLC separated fractions and their difference spectra (a4) confirm the full disappearance of F-related peaks upon trypsin digestion. (b1) Raman and SERS spectra of the CALNYYGGGGNNE trypsin substrate with characteristic tryptophan peaks. (b2) RP-HPLC and mass spectrometry analysis after incubation with endoprotease Glu-C show almost complete digestion after 4 hours of incubation. (b3 and b4) The SERS spectra and difference spectrum of the RP-HPLC separated fractions show the disappearance of the tryptophan-related peaks after cleavage. ‡

Table 1 Peak assignment of the Raman and SERS spectra of the CALNNYGGGGVGRGNF peptide. The Raman spectrum of the short peptide CALNN was separately measured. The SERS peaks marked in bold will decrease upon trypsin activity

Raman (cm ⁻¹)	SERS (cm ⁻¹)	Origin	Raman	SERS	Origin
621	618	F ¹⁸	1126	1124	G ³⁷ , CALNN
642	—	Y ¹⁸ , CALNN	1176	1178	Y ³⁷
723	730	CALNN	1207	1206	F ¹⁸
834	829	Y ¹⁸	1229	1240	Amide IIIβ ³⁷
853	860	Y ¹⁸ , A ³⁷	1325	1330	G ³⁷
898	889	G ³⁷	1429	1426	CALNN
957	948	CALNN	—	1448	G ³⁷
1003	1003	F ^{18,37}	1607	1603	CALNN
1031	1030	F ^{18,37} , CALNN	1674	1677	Amide I ³⁷

Hydrolysis of unbound peptides observed through SERS spectra of HPLC separated fractions

Fig. 4(a1 and b1) compare the spontaneous Raman- to SERS-spectra of CALNNYGGGGVGRGNF (trypsin substrate) and CALNNYGGGGNNESWH (endoproteinase Glu-C substrate) peptides labelled on a nanodome platform. Their respective Raman bands are identified in Tables 1 and 2 based on the SERS^{18,19} and Raman^{37,38} spectra of amino acids reported in the literature and on our own measurements of the peptide CALNN. We are particularly interested in the peaks selective for the peptide products that are either cleaved off or remain on the surface. These include the 1003 cm⁻¹ symmetric bending mode of phenylalanine (F) *versus* the 833 cm⁻¹ in plane and 853 cm⁻¹ out plane ring breathing modes of tyrosine (Y), and the symmetric benzene/pyrrole in-phase breathing mode of tryptophan (W) at 760 cm⁻¹.¹⁸

As a first step, we monitored the activity of the protease on the substrate in solution. RP-HPLC was used to separate the substrate from the digestion products, which are subsequently labelled on a nanodome platform. From the difference spectrum, we derive the characteristic peaks of the cleaved-off and

Table 2 Peak assignment for the CALNNYGGGGNNESWH peptide for endoproteinase Glu-C digestion. The SERS peaks marked in bold will decrease upon endoproteinase Glu-C activity

Raman (cm ⁻¹)	SERS (cm ⁻¹)	Origin	Raman	SERS	Origin
642	642	Y ¹⁸ , CALNN	—	1118	W ³⁷
723	—	CALNN	1176	1177	Y ³⁷
758	754	W ^{18,37,38}	1232	1235	W ^{37,38}
832	—	Y ¹⁸	1257	—	W ³⁷ , H ³⁷
852	—	Y ¹⁸ , A ³⁷	1361	1356	W ^{18,37,38}
—	868	?	1430	1423	CALNN, W ³⁷
879	—	W ^{18,37,38}	—	1535	?
893	—	G ³⁷	1552	—	W ^{18,37,38}
—	999	?	—	1602	CALNN
1012	—	W ^{18,37}	1618	—	W ³⁷ , G ³⁷ , CALNN
1030	1027	CALNN	1672	1674	Amide I ³⁹

remaining fractions. Fig. 4(a2–a4) depicts the results of this experiment for trypsin and its CALNNYGGGGVRRGNF ($100 \mu\text{g ml}^{-1}$) substrate. The peptide was incubated with trypsin ($3.3 \mu\text{g ml}^{-1}$) at a 1/30 (w/w) ratio in a 50 mM ammonium-bicarbonate (pH 7.8) buffer in water, and separated with RP-HPLC (Fig. 4(a2)) after 0, 30 and 90 minutes of incubation. The RP-HPLC-separated peptides and their fragments were identified using MALDI-TOF mass spectrometry. Prior to adding trypsin, we found two fractions; one corresponding to an uncleaved monomer and the other to an uncleaved dimer. The dimer formation is a consequence of the oxidation of the cysteine thiol groups upon which a disulphide bond is formed between two peptides. The substrate was almost fully digested after 30 minutes and transformed into cleaved monomer, single cleaved dimer and double cleaved dimer fractions. After 90 minutes, the peptides were found to be fully cleaved. Subsequently, we labelled the nanodome chips with cleaved and uncleaved fractions. The resulting SERS spectra (Fig. 4(a3 and a4)†) show full disappearance of the 1003 cm^{-1} peak in the cleaved fraction. Furthermore, the peaks at 618 cm^{-1} , 1030 cm^{-1} and 1207 cm^{-1} show a partial decrease, although their signal to noise ratio is low. All these peaks correspond to those attributed to phenylalanine (Table 1). From this experiment, we conclude that the ratio between the 1003 cm^{-1} peak and the $829\text{--}860 \text{ cm}^{-1}$ peaks ($I_{1003}/I_{829-860}$) is a correct metric for I_F/I_Y , the cleavage of the substrate by trypsin.

Fig. 4(b2–b4) describes an analogous experiment for endoproteinase Glu-C ($3.3 \mu\text{g ml}^{-1}$) and its CALNNYGGGGNNESWH ($100 \mu\text{g ml}^{-1}$) substrate. Peptide digestion was slightly less efficient, with almost full conversion of the substrate to products only after 4 hours of incubation. Because of the large adsorption of tryptophan at 270 nm and its strong interaction with the RP-HPLC resin, the –SWH product is also visible as a separate fraction. After binding the cleaved peptide and uncleaved dimer to the nanodome chips, we observed a disappearance of the 754 cm^{-1} and 1356 cm^{-1} peaks upon cleavage, as well as a reduction of the contributions at the 999, 1118 and 1531 cm^{-1} peaks. These changes correspond to the peak assignments shown in Table 2, but more experiments are needed for an improved peak assignment of the CALNNYGGGGNNESWH substrate.

Hydrolysis of unbound peptides observed through SERS spectra of a non-separated mixture

Apart from a thiol–gold interaction, N-terminal primary amines can also lead to a charge-based adsorption on metal surfaces.⁴⁰ This effect may be additive in the case of cysteine, but could lead to the adsorption of unwanted amino acids on the gold surface. In a second set of in-solution experiments, we ran a similar trypsin – CALNNYGGGGVRRGNF assay without separating the fractions by RP-HPLC (Fig. 5). One nanodome chip was labelled with a reference solution of the peptide ($100 \mu\text{g ml}^{-1}$), another with a solution of peptide ($100 \mu\text{g ml}^{-1}$) and trypsin ($2 \mu\text{g ml}^{-1}$) after 2 hours of incubation. The lack of a phenylalanine peak at 1003 cm^{-1} in the trypsin-incubated solution confirms that the peptide had been fully digested and

† The appearance of some new peaks in the fractions in Fig. 4(a3 and b3) compared to the spectra acquired in Fig. 4(a1 and b1) is attributed to unknown sources of contamination during the HPLC separation. For example, the newly appearing peaks in the cleaved fraction CALNNYGGGGVRR at 747 , 1540 and 1603 cm^{-1} did not appear in other experiments on this peptide.

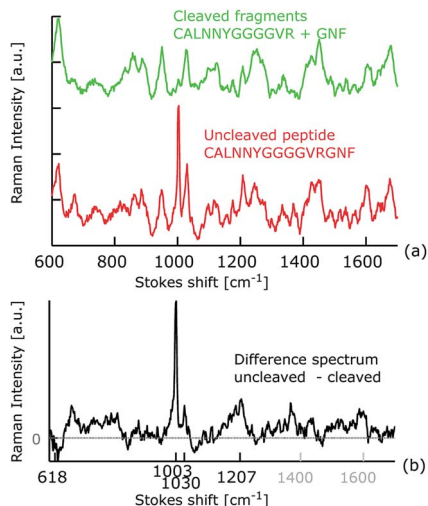


Fig. 5 (a) SERS spectra of a peptide solution before (red) and after (green) trypsin incubation prove that the binding of the peptide to the gold surface happens via the side-chain of the N-terminal cysteine through a gold–sulphur bond, but not via the free amine part of the –GNF product. (b) The difference spectrum before and after cleavage agrees with the difference between the RP-HPLC separated uncleaved and cleaved fractions shown in Fig. 4.

that the products bind to the surface through the thiol side-chain on the cysteine, but not through charge-based adsorption of the free amine group on the –GNF cleaved off product. Furthermore, the SERS and difference SERS-spectra shown in Fig. 5 confirm the findings of the RP-HPLC experiment in Fig. 4(a).

SERS-monitored trypsin hydrolysis of gold-nanodome bound peptides

In a third experimental setup, three CALNNYGGGGVRGNF labelled nanodome chips were incubated in a buffer without trypsin, with trypsin and with trypsin plus an ovomucoid inhibitor for 45 minutes (Fig. 6). The chip incubated with trypsin plus inhibitor shows a SERS spectrum resembling that of the reference chip, suggesting a full blockade of tryptic cleavage by the ovomucoid inhibitor. On the chip with trypsin only, the surface bound peptides are cleaved, resulting in a decrease of $I_{1003}/I_{829-860}$ by 40–48%. Full disappearance of the –GNF fingerprint was never observed, at most $I_{1003}/I_{829-860}$ decreased by 53% over all our experiments. We consider two possible origins for the remaining signal at 1003 cm⁻¹. One is a partial re-adsorption of the –GNF products on the gold surface; the tripeptides that do not diffuse out of the hotspot region will continue contributing to the SERS spectrum. However, the experiment in Fig. 5 suggests this is not the case. More likely, the remaining signal originates from the peptides that are not accessible to the protease due to steric hindrance. This can be a result of having a too dense monolayer of peptides^{11,23} or due to inaccessible parts of the nanodome geometry. Especially in the latter case, the inaccessible peptides are probably located in the nanodome gaps and will contribute disproportionately strongly to the SERS signal. Thus, it is plausible that significantly more than 53% of the protease-accessible peptides has been cleaved.

The difference spectrum in Fig. 6(c) shows exactly the same features as those observed upon bulk digestion followed by SERS labelling in Fig. 4(a4) and 5(c). Furthermore, we did not observe significant differences in the absolute strength of the CALNNYGGGGVR fingerprint, which shows that the ligand exchange was limited in this assay. Ligand exchange is more prominent in a reducing environment, in which a reduction of the gold–sulphur bond results in a detachment of the peptides. These reductive environments are present in cells and are of particular importance for the activation of cysteine proteases. While normalization to the trypsin peaks at 833–853 cm^{-1} is not strictly necessary in this case, it

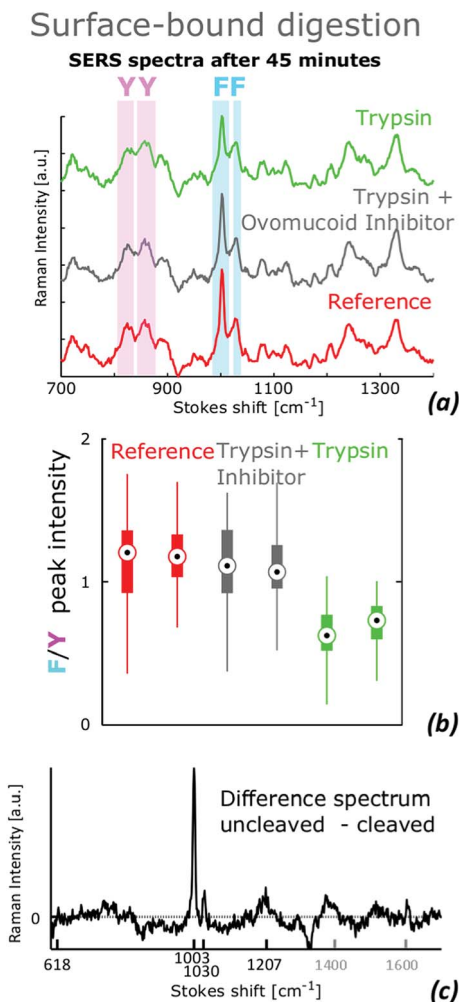


Fig. 6 Trypsin cleavage of the surface-bound CALNNYGGGGVRGNF peptides. (a) SERS spectra with the characteristic tyrosine and phenylalanine peaks highlighted in blue and pink. (b) Relative intensity of the highlighted peaks (I_F/I_Y), showing peptide cleavage in the presence of trypsin which is blocked when an ovomucoid (type II-O) inhibitor is added. (c) Difference spectrum between the sample with and without trypsin, which agrees well with the results of the bulk digestion in Fig. 4 and 5.

does provide an inherent correction for differences in the acquisition parameters such as laser power or focus drift as well as limited variations across the SERS platform.

Real time observation of trypsin activity

Finally, CALNNYGGGVRGNF labelled chips were incubated with trypsin under the Raman microscope for real-time acquisition of the SERS spectra. Fig. 7(a) shows the evolution of these spectra before and after trypsin addition. A new spectrum was acquired every 2–3 minutes with an integration time of 100 seconds. A relative decrease of I_{1003} versus the peaks at 829, 860, 948, 1248, 1330, 1603 and 1677 cm^{-1} is visible within the first minutes after adding 0.2 $\mu\text{g ml}^{-1}$ trypsin (8.6 nM) to a total volume of 1 ml (8.6 pmol), in agreement with Table 1 and the earlier experiments described in this work. The SERS spectra after 2 minutes and 30 minutes of trypsin incubation show a further reduction of I_{1003} and I_{1206} with increasing incubation time (Fig. 7(b)). The fast decrease of $I_{1003}/I_{829-860}$ in the first minutes after trypsin addition demonstrates that at trypsin concentrations ranging from 1 to 0.2 $\mu\text{g ml}^{-1}$, most of the accessible substrate was cleaved within the time-span of the first measurement (Fig. 7(c)). The curves of $I_{1003}/I_{829-860}$ versus time qualitatively agree to the kinetics of enzymatic reactions on self-assembled monolayers.^{41,43} Remarkably, the SERS spectra suggest that the cleavage rate is similar for 0.2, 0.5 and 1 $\mu\text{g ml}^{-1}$ trypsin. We assume that even for the lowest trypsin concentration, a limiting velocity for cleavage of the surface-bound peptides in the plasmonic hotspots is reached. The enzyme kinetics on immobilized substrates can be substantially different from those on substrates in solution. The latter follow Michaelis–Menten kinetics under the assumption of an excess substrate concentration. On the nanodome surface this is no longer valid because of the very low concentration of immobilized substrates, therefore a further increase in the enzyme concentration does not increase the initial cleavage rate.⁴³

More measurements are required to support this assumption and accurately determine the trypsin detection limit and on-chip enzyme kinetics, especially in the first minutes after trypsin incubation.

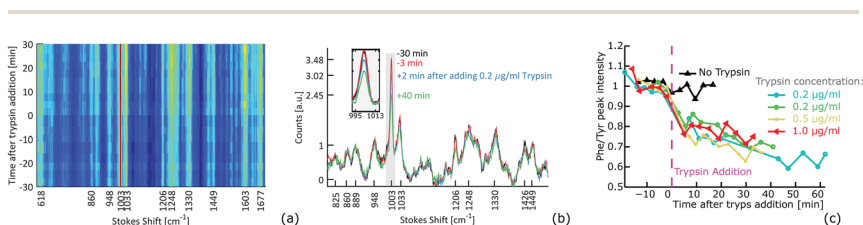


Fig. 7 Real-time trypsin digestion of gold-nanodome bound peptides. (a) Evolution of the SERS spectra before and after trypsin addition, scaled for equal 1003 cm^{-1} intensity. This shows a relative increase of the CALNNYGGGVR-related peaks at 829, 860, 948, 1248, 1330, 1603 and 1677 cm^{-1} versus the 1003 cm^{-1} phenylalanine peak upon trypsin addition ($t = 0$). (b) SERS spectra at individual time points, the inset zooms in on the 1003 cm^{-1} F-peak. (c) Time evolution of $I_{1003}/I_{829-860}$, characterized by $I_{1003}/I_{829-860}$ and measured in four different experiments, all showing a fast cleavage within the first minutes after trypsin addition.

Experimental

Materials

para-Nitrothiophenol (4-NTP, Sigma N27209), endoproteinase Glu-C (*Staphylococcus aureus* V-8 protease, Thermofisher 20195), sequencing grade modified trypsin (Promega V5111), *N*- α -benzoyl-DL-arginine 4-nitroanilide hydrochloride (*L*-BAPNA, Sigma B4875), ovomucoid (type II-O) trypsin inhibitor from chicken egg white (Sigma, T9253), monodisperse polystyrene microbeads (microparticles GmbH, 448 nm), dichloromethane (Sigma), dimethylformamide (Sigma), ammonium bicarbonate (Sigma), acetonitrile (Sigma), acetone (VWR), isopropyl alcohol (VWR), ethanol (Anhydrous, Sigma), methanol (VWR), sulfuric acid (VWR), and hydrogen peroxide (VWR).

Finite difference time domain simulations

Lumerical FDTD solutions® was used for simulating the field profile in the plasmonic hotspots. A total-field scattered-field source (TFSE) is incident on a gold nanodome dimer in water on a Si₃N₄/Si substrate with a 224 nm radius and 10 nm gap width with anti-symmetric, PML and symmetric boundaries along respectively X, Y and Z. All geometrical parameters were set to match the data from the SEM top view and cross-section images to the best of our ability. The refractive indices are set as follows: $n_{\text{SiN}} = 2$, $n_{\text{Au}} = \text{ref. 42}$, and $n_{\text{water}} = 1.33$.

Peptide synthesis

The peptides were synthesized using standard solid-phase Fmoc chemistry on a SyroI (biotage) instrument. The synthesis was started on 25 μmol preloaded Fmoc-His(Trt) or Fmoc-Phe wang resin respectively (Novabiochem). The amino acids were coupled in a 4-fold excess using HOBT/HBTU activation. The peptides were cleaved with TFA containing phenol, triisopropylsilane and 5% H₂O for 3 hours. The peptides were precipitated with tributylmethyl ether and recovered by centrifugation at 2000g. The ether washing/centrifugation step was repeated 3 times. The peptides were purified using a water/acetonitrile gradient elution on a RPC C18 column (Macherey-Nagel).

Peptide assays

Peptides were first dissolved to 100 $\mu\text{g ml}^{-1}$ in DMF and further diluted to 100 $\mu\text{g ml}^{-1}$ in either a 10% acetonitrile/water mixture for labelling or a 50 mM ammonium bicarbonate buffer (pH 7.8) for bulk digestion experiments. Prior to labelling the chips with the peptides, they were cleaved into pieces of a few mm^2 and cleaned by sonication in acetone, rinsed with isopropylalcohol and water and dried with under a stream of nitrogen. Next, the remaining organic contaminants were removed in an O₂ plasma, which also renders the surface hydrophilic (120 s, PVA-TEPLA GIGA batch 310 M, 6000 sccm O₂, 600 W, 750 mTorr). Immediately afterwards, the chips were immersed in separate wells of a polypropylene 96-well plate, using 100 μl of a 100 $\mu\text{g ml}^{-1}$ peptide solution in 10% acetonitrile in water. After overnight incubation, the chips were rinsed excessively with deionized water. All assays were done in a freshly prepared 50–100 mM ammonium-bicarbonate buffer at 37 °C. Both trypsin and endoproteinase Glu-C were first

incubated at 37 °C for 15 min prior to addition to the peptide substrate, ensuring immediate maximal enzyme activity. The effectivity of the ovomucoid trypsin inhibitor for blocking trypsin digestion was tested in a 405 nm absorption assay (Tecan Infinite 200 PRO) on the commercially available L-BAPNA trypsin substrate. We used an excessive inhibitor concentration of 100 $\mu\text{g ml}^{-1}$.

HPLC and mass spectrometry

After incubation for a specific time at 37 °C, 750 μl of a solution with 100 $\mu\text{g ml}^{-1}$ substrate and 3.3 $\mu\text{g ml}^{-1}$ trypsin or endoproteinase Glu-C in 50–100 mM ammonium bicarbonate was injected in a C-18 reversed phase high-performance liquid chromatography column (Macherey-Nagel) and eluted by a water/acetonitrile gradient (Äkta Purifier, GE). The molecular weight of the separated fractions was determined using matrix-assisted laser desorption/ionisation time-of-flight mass spectrometry (Brüker MALDI-TOF).

Raman microscopy

The spectra were acquired on a WITec Alpha 300R+ confocal Raman microscope equipped with a spectrometer using a 600 lpm grating, a -70 °C cooled CCD camera (Andor iDus 401 BR-DD) and a 785 nm diode laser (Toptica, XTRA II). The Raman spectra of the peptide powders were acquired using a Zeiss 100 \times /0.9 EC Epiplan NEOFLUAR; $\infty/0$ objective and a laser power of 100 mW, measured before the objective. The SERS spectra were acquired through a Zeiss 63 \times /1.0 W-Plan Apochromat $\infty/0$ objective with a 2 mW laser power. For real-time monitoring of enzymatic activity, the chip was placed in a metal Petri dish filled with 1 ml of 50 mM ammonium bicarbonate buffer (pH 7.8) inside a stage-top incubator at 37 °C (Okolab). Because of the signal degradation upon laser illumination, each trace is the median spectrum of a spatially distributed map of 10 \times 10 pixels in a 20 \times 20 μm area with an integration time of 1 s on each point. In the real-time assay, every next trace was mapped on a different location on the SERS platform. A limited amount of anisotropy across the gold nanodome area accounts for the variation in $I_{1003}/I_{829-860}$ visible in Fig. 7(c).

SERS data processing

Starting from the 10 \times 10 individual spectra, WITec Project Four® was used for removing cosmic rays. Next, the data was exported to Matlab® and aberrant spectra were rejected using a variance-based filter, after which the background of each individual spectrum is subtracted using a high-pass filter. All SERS spectra plotted in this paper are the median spectra of these data. I_{1003} and $I_{829-860}$ were calculated by integrating the peaks at their respective positions and subtracting the background with a linear fit for the individual spectra. The boxplots in Fig. 6 are based on these individual peak intensities.

SERS enhancement factor calculations

After cleaning, the chips were immersed overnight in a 1 mM solution of 4-NTP in ethanol and rinsed excessively in ethanol. The SERS³⁶ substrate enhancement factor is calculated from the ratio between the Raman signal per molecule in a bulk solution ($\rho = 100$ mM in ethanol, 10 \times /0.3 Nikon PlanFluor objective, 100

mW, 0.13 s) and the SERS signal per adsorbed molecule on the nanodome surface ($10\times/0.3$ Nikon PlanFluor objective, 0.1 mW, 0.13 s):

$$\text{SSEF} = \frac{I_{\text{SERS}} N_{\text{Vol}}}{I_{\text{Raman}} N_{\text{Surf}}} = \frac{I_{\text{SERS}}}{I_{\text{Raman}}} \frac{H_{\text{eff}} \rho}{\mu_{\text{Au}} \mu_{\text{NTP}} A_{\text{m}}}$$

For this calculation, we used an effective height (H_{eff}) of the confocal volume of 160 μm , a factor of 1.6 for the ratio of the nanodome surface area over projected surface area ($\mu_{\text{Au}} A_{\text{m}}$) and a loading density (μ_{NTP}) of 4.4×10^6 molecules per μm^2 .⁴⁴

Nanodome fabrication

4" wafers patterned with nanodome substrates were fabricated by optimizing an earlier published protocol,²¹ as schematically shown in Fig. 2(a). First, a 200 nm layer of PECVD Si_3N_4 was deposited on top of a 4" (100) Si wafer (Advanced Vacuum Vision 310-PECVD). Next, the wafer was cleaned and made hydrophilic by 20 min of O_2 plasma (PVA-TEPLA GIGA batch 310 M, 6000 sccm O_2 , 600 W, 750 mTorr) and stored in DI water. Prior to spincoating, the wafer was flash-dried under a stream of nitrogen, followed by spincoating 760 μl of a 5 w/v% in 2/1 methanol/water mixture of 448 nm diameter polystyrene beads on top of the wafer. The exact spin speed and acceleration depend on environmental parameters such as humidity and temperature. Typically, a two-step process was used, first generating the hexagonally-packed monolayer by spinning at 900 rpm and with an acceleration of 800 rpm s^{-1} for 100 s, followed by faster spinning at 7000 rpm for 40 s to remove excess beads and solvent, and finally again flash-drying the wafer with nitrogen. The HCP-layer of the polystyrene beads was then transferred into the underlying Si_3N_4 using a two-step reactive ion etch. First, the diameter of the beads was reduced in an O_2 plasma (Advanced Vacuum Vision 320-RIE, 50 sccm O_2 , 75 W, 100 mTorr, 40–70 s), followed by a CF_4/H_2 Si_3N_4 etch using an optimised recipe for anisotropic etching (80 sccm CF_4 , 3 sccm H_2 , 210 W, 20 mTorr, 70–100 s). These two steps respectively determine the width and height of the gap in between the nanodomains, the two most important parameters for tuning the plasmonic resonance, enhancement factor and hot-spot accessibility. Next, the beads were lifted off in dichloromethane and the wafers were cleaned in a piranha solution ($\text{H}_2\text{SO}_4/\text{H}_2\text{O}_2$, 3/1, 15 minutes at 80 $^\circ\text{C}$) before sputtering of a 2 nm thick Ti adhesion layer and a 130 nm thick Au layer (Alcatel SCM600, 10^{-2} mbar, 1 kW, rotating substrates). The chips were characterized through scanning electron microscopy on a FEI Nova 600 Nanolab Dual-Beam FIB system, using a voltage of 18 kV and through the lens (TLD) detection.

Conclusions

We successfully used SERS to monitor the protease-catalysed hydrolysis of a peptide made from just natural amino acids using the Raman fingerprint of aromatic amino acids. The peptide CALNYYGGGGVVRGNF forms a stable monolayer of trypsin substrates on a gold-nanodome platform, whose plasmonic hot-spots are accessible to proteases of 20–30 kDa. Real-time monitoring of trypsin activity on this gold-bound peptide shows immediate digestion within the first

two minutes for a 8.6 nM concentration. We further demonstrate that an analogous peptide sequence CALNNYGGGGNNESWH provides a good substrate for endoprotease Glu-C and identify the SERS spectra of both the substrates and their products, thereby taking a first step towards a label-free multiplexed measurement of protease activity. We are working on further quantification of the enzyme activity on gold-nanodome bound substrates for single and multiplexed protease activity. The 8.6 nM concentration of trypsin used in this paper is not yet among the lowest detectable protease concentrations reported. Although we have not fully studied the sensitivity of our assay, a detection limit in the pM range^{11,14} is unlikely in the current setup. Options to increase the sensitivity include reducing the substrate density using a matrix peptide²³ or selectively labelling the hotspots. Also, the assay presented in this work has not yet been tested in realistic *in vitro* conditions, where non-specific cleavage or ligand exchange may complicate the measurement. We expect that our ratiometric measurement will be an important asset in these conditions. Possibly more stable monolayers using a double cysteine²² or alkanethiol-PEG⁴⁵ chains will be required in these cases. In summary, the important advantages of the real-time detection of protease activity presented in this manuscript over existing SERS-based techniques are the completely label-free measurements and the inherent control against ligand exchange. Furthermore we use a nanosphere-lithography based SERS platform that offers controllable hotspots and is relatively easy and cheap to fabricate. In combination with microfluidics, SERS-based microchips can offer a promising platform for a sensitive, selective and multiplexed measurement of protease activity in various applications.

Acknowledgements

P. W. and N. T. acknowledge the Research Foundation Flanders (FWO) for predoctoral fellowships. A. G. S. acknowledges BOF UGent (MRP B/11267/10) and FWO (FWOOPR2013010502) for financial support. R. B., P. W. and N. T. acknowledge the InSpectra ERC Advanced Grant (7336509).

Notes and references

- 1 M. Drag and G. S. Salvesen, *Nat. Rev. Drug Discovery*, 2010, **9**, 690–701.
- 2 B. Turk, *Nat. Rev. Drug Discovery*, 2006, **5**, 785–799.
- 3 K. Y. Choi, M. Swierczewska, S. Lee and X. Chen, *Theranostics*, 2012, **2**, 156–179.
- 4 M. Wu and A. K. Sing, *Curr. Opin. Biotechnol.*, 2012, **23**, 83–88.
- 5 T. Liu, Y. Yamaguchi, Y. Shirasaki, K. Shikada, M. Yamagishi, K. Hoshino, T. Kaisho, K. Takemoto, T. Suzuki, E. Kuranaga, O. Ohara and M. Miura, *Cell Rep.*, 2014, **8**, 974–982.
- 6 D. Maysinger and E. Hutter, *Nanomedicine*, 2015, **10**, 483–501.
- 7 Y.-P. Kim and H. S. Kim, *ChemBioChem*, 2016, **17**, 275–282.
- 8 K. Welser, R. Adsley, B. M. Moore, W. C. Chan, J. W. Aylott and C. Chan, *Analyst*, 2011, **136**, 29–41.
- 9 Y. Lai, S. Sun, T. He, S. Schlücker and Y. Wang, *RSC Adv.*, 2015, **5**, 13762–13767.
- 10 G. L. Liu, Y. T. Rosa-Bauza, C. M. Salisbury, C. Craik, J. a. Ellman, F. F. Chen and L. P. Lee, *J. Nanosci. Nanotechnol.*, 2007, **7**, 2323–2330.

- 11 C. Sun, K. H. Su, J. Valentine, Y. T. Rosa-Bauza, J. A. Ellman, O. Elboudwarej, B. Mukherjee, C. S. Craik, M. A. Shuman, F. F. Chen and X. Zhang, *ACS Nano*, 2010, **4**, 978–984.
- 12 C. Fu, W. Xu, G. Chen and S. Xu, *Analyst*, 2013, **138**, 6282–6286.
- 13 L. Chen, X. Fu and J. Li, *Nanoscale*, 2013, **5**, 5905–5911.
- 14 Z. Wu, Y. Liu, Y. Liu, H. Xiao, A. Shen, X. Zhou and J. Hu, *Biosens. Bioelectron.*, 2015, **65**, 375–381.
- 15 A. Ingram, L. Byers, K. Faulds, B. D. Moore and D. Graham, *J. Am. Chem. Soc.*, 2008, **130**, 11846–11847.
- 16 I. A. Larmour, K. Faulds and D. Graham, *Chem. Sci.*, 2010, **1**, 151–160.
- 17 B. D. Moore, L. Stevenson, A. Watt, S. Flitsch, N. J. Turner, C. Cassidy and D. Graham, *Nat. Biotechnol.*, 2004, **22**, 1133–1138.
- 18 F. Wei, D. Zhang, N. J. Halas and J. D. Hartgerink, *J. Phys. Chem. B*, 2008, **112**, 9158–9164.
- 19 E. Jorgenson and A. Ianoul, *J. Phys. Chem. B*, 2017, **121**, 967–974.
- 20 R. Lévy, N. T. K. Thanh, R. Christopher Doty, I. Hussain, R. J. Nichols, D. J. Schiffrin, M. Brust and D. G. Fernig, *J. Am. Chem. Soc.*, 2004, **126**, 10076–10084.
- 21 P. C. Wuytens, A. Z. Subramanian, W. H. De Vos, A. G. Skirtach and R. Baets, *Analyst*, 2015, **140**, 8080–8087.
- 22 V. See, P. Free, Y. Cesbron, P. Nativo, U. Shaheen, D. J. Rigden, D. G. Spiller, D. G. Fernig, M. R. H. White, I. A. Prior, M. Brust, B. Lounis and R. Levy, *ACS Nano*, 2009, **3**, 2461–2468.
- 23 P. Free, C. P. Shaw and R. Levy, *Chem. Commun.*, 2009, **33**, 5009–5011.
- 24 S. S. Masango, R. A. Hackler, N. Large, A. I. Henry, M. O. McAnally, G. C. Schatz, P. C. Stair and R. P. Van Duyne, *Nano Lett.*, 2016, **16**, 4251–4259.
- 25 M. Gellner, K. Kömpe and S. Schlücker, *Anal. Bioanal. Chem.*, 2009, **394**, 1389–1844.
- 26 E. Colangelo, Q. Chen, A. M. Davidson, D. Paramelle, M. B. Sullivan, M. Volk and R. Levy, *Langmuir*, 2017, **33**, 438–449.
- 27 H. Häkkinen, *Nat. Chem.*, 2012, **4**, 443–455.
- 28 L. Duchesne, D. Gentili, M. Comes-Franchini and D. G. Fernig, *Langmuir*, 2008, **24**, 13572–13580.
- 29 E. Vandermarliere, M. Mueller and L. Martens, *Mass Spectrom. Rev.*, 2013, **32**, 453–465.
- 30 M. Pozsgay, G. Szabó, S. Bajusz, R. Simonsson, R. Gáspár and P. Elödi, *Eur. J. Biochem.*, 1981, **115**, 497–502.
- 31 K. Breddam and M. Meldal, *Eur. J. Biochem.*, 1992, **206**, 103–107.
- 32 H. P. Erickson, *Biol. Proced. Online*, 2009, **11**, 32–51.
- 33 L. Bayne, R. V. Ulijn and P. J. Halling, *Chem. Soc. Rev.*, 2013, **42**, 9000–9010.
- 34 E. Le Ru and P. Etchegoin, *Principles of Surface Enhanced Raman Spectroscopy and related plasmonic effects*, Elsevier, 2009, vol. 1.
- 35 A. Yashchenok, A. Masic, D. Gorin, B. S. Shim, N. A. Kotov, P. Fratzl, H. Möhwald and A. Skirtach, *Small*, 2013, **9**, 351–356.
- 36 E. C. Le Ru, M. Meyer and P. G. Etchegoin, *J. Phys. Chem. C*, 2007, **111**, 13794–13803.
- 37 J. De Gelder, K. De Gussem, P. Vandenabeele and L. Moens, *J. Raman Spectrosc.*, 2007, **38**, 1133–1147.

- 38 G. Zhu, X. Zhu, Q. Fan and X. Wan, *Spectrochim. Acta, Part A*, 2011, **78**, 1187–1195.
- 39 Z. Movasaghi, S. Rehman and I. U. Rehman, *Appl. Spectrosc. Rev.*, 2007, **42**(5), 493–541.
- 40 J. Zhang, Q. Chi, J. U. Nielsen, E. P. Friis, J. E. T. Andersen and J. Ulstrup, *Langmuir*, 2000, **16**, 7229–7237.
- 41 S. Nayak, W. Yeo and M. Mrksich, *Langmuir*, 2007, **17**(2), 5578–5583.
- 42 P. B. Johnson and R. W. Christy, *Phys. Rev. B*, 1972, **6**, 4370–4379.
- 43 O. A. Gutiérrez, M. Chavez and E. Lissi, *Anal. Chem.*, 2004, **76**, 2664–2668.
- 44 L. Baia, M. Baia, J. Popp and S. Astilean, *J. Phys. Chem. B*, 2006, **110**, 23982–23986.
- 45 R. Derda, D. J. Wherritt and L. L. Kiessling, *Langmuir*, 2007, **23**, 11164–11167.